Journal of Materials Research and Technology 36 (2025) 7261–7273

Contents lists available at ScienceDirect

Journal of Materials Research and Technology

journal homepage: www.elsevier.com/locate/jmrt

Innovative mortars containing nanofibrillated cellulose (NFC) and basic oxygen furnace slag (BOFS): optimizing ultrasonication methods for higher eco-efficiency

Rodrigo Felipe Santos [a], José Carlos Lopes Ribeiro [b], José Maria Franco de Carvalho [b], Washington Luiz Esteves Magalhães [d], Leonardo Gonçalves Pedroti [b], Gustavo Henrique Nalon [b], Gustavo Emilio Soares de Lima [b], Eduardo Nery Duarte de Araújo [c], Afonso Rangel Garcez de Azevedo [e,*]

[a] Department of Engineering and Computing, Santa Cruz State University, Campus Soane Nazaré de Andrade, Rodovia Jorge Amado, km 16, Bairro Salobrinho, Ilhéus, Bahia, 45.662-900, Brazil
[b] Department of Civil Engineering, Federal University of Viçosa, Av. Peter Henry Rolfs, Campus UFV, Viçosa, Minas Gerais, 36.570-900, Brazil
[c] Department of Physics, Federal University of Viçosa, Av. Peter Henry Rolfs, Campus UFV, Viçosa, Minas Gerais, 36.570-900, Brazil
[d] Brazilian Agricultural Research Corporation - Forestry (Embrapa Forestry), Estrada da Ribeira, Km 111, Guaraituba, Colombo, Paraná, 83411-000, Brazil
[e] Department of Civil Engineering, Universidade Estadual do Norte Fluminense Darcy Ribeiro, Av. Alberto Lamego, 2000, Parque Califórnia, Campos dos Goytacazes, Rio de Janeiro, 28013-602, Brazil

ARTICLE INFO

Handling editor: M Meyers

Keywords:
Dispersion of nanomaterials
Nanofibrillated celluloses
Steel slag
Cement-based composites
Eco-efficiency

ABSTRACT

Incorporating waste materials into cementitious composites is a promising practice for enhancing the sustainability of the construction industry. However, previous papers have not explored the combination of nanofibrillated cellulose (NFC) with basic oxygen furnace slag (BOFS) for producing eco-efficient mortars, nor have they examined the optimization of NFC dispersion within these matrices. To narrow these research gaps, this paper presents an experimental program for the design of innovative mortars containing both NFC and BOFS, based on the optimization of ultrasonication procedures for improvement of eco-efficiency indicators. Ultraviolet–visible (UV–vis) spectroscopy, zeta potential analysis, and scanning electron microscopy (SEM) were used to evaluate the dispersion and stability of NFC solutions prepared with different sonication times (0.00, 0.04, 0.08, 0.16, and 0.32 min/ml). Mortars containing BOFS and these different types of NFC solutions were subjected to tests for determination of workability, compressive strength, flexural strength, eco-efficiency indicators, X-ray diffraction (XRD) and SEM analyses. Results indicated improved NFC dispersion and stability through sonication, leading to enhanced mechanical performance and eco-efficiency indicators. The most favorable results were observed in mortars with NFC sonication times of 0.04 and 0.16 min/ml, showcasing performance gains of 17.9 % and 13.4 % compared to the reference specimen, respectively. In conclusion, optimizing ultrasonication methods can be a highly effective strategy for enhancing the eco-efficiency performance of novel mortars containing BOFS and NFC.

1. Introduction

Recently, there has been an increasing focus on seeking sustainable alternatives for diverse services and products. This trend has notably impacted industries that place significant pressure on the environment. In particular, the construction industry stands out as a major consumer of natural resources such as rocks, metals, wood, and water. It is also a substantial energy consumer, a significant waste producer, and a major contributor to greenhouse gas emissions [1,2].

To mitigate environmental impacts and decrease the extraction of natural resources, natural aggregates of cementitious composites can be replaced with waste materials. Numerous studies have demonstrated the viability of utilizing construction and demolition waste [3–5], mining

* Corresponding author.
E-mail addresses: rfsantos@uesc.br (R.F. Santos), jcarlos.ribeiro@ufv.br (J.C.L. Ribeiro), josemaria.carvalho@ufv.br (J.M. Franco de Carvalho), washington.magalhaes@embrapa.br (W.L.E. Magalhães), leonardo.pedroti@ufv.br (L.G. Pedroti), gustavo.nalon@ufv.br (G.H. Nalon), gustavo.lima@ufv.br (G.E.S. Lima), eduardo.araujo@ufv.br (E.N.D. Araújo), afonso@uenf.br (A.R.G. Azevedo).

https://doi.org/10.1016/j.jmrt.2025.04.319
Received 29 January 2025; Received in revised form 17 April 2025; Accepted 30 April 2025
Available online 1 May 2025
2238-7854/© 2025 The Authors. Published by Elsevier B.V. This is an open access article under the CC BY-NC-ND license (http://creativecommons.org/licenses/by-nc-nd/4.0/).

Abbreviations and symbols:

BOFS	basic oxygen furnace slag
CNC	cellulose nanocrystals
CNT	carbon nanotube
DLS	Dynamic Light Scattering
NFC	nanofibrillated cellulose
SCD	short-circuit diffusion
SP	superplasticizer
UV–vis	Ultraviolet visible
CI_c -	cement intensity for compressive strength
CI_f -	cement intensity for flexural strength
N	number of samples
c -	total cement consumption
p_c -	composite performance in compression
p_f -	composite performance in bending

residues [6–8], agricultural waste [9–11], and metallurgy wastes [12–14] for this purpose. For example, basic oxygen furnace slag (BOFS), which originates from steel production utilizing the Linz-Donawitz process, deserves particular attention. Produced on a large scale by the steel industry [15,16], BOFS primarily consists of four oxides: lime (CaO), periclase (MgO), silica (SiO_2), and wustite (FeO) [17]. Utilizing BOFS as aggregates for concrete production offers the advantage of diminishing the extraction of rocks and sand from natural sources while offering a suitable disposal solution for industrial residues. Furthermore, the mechanical strength of BOFS aggregates is comparable to or even higher than that of conventional aggregates [18]. BOFS also presents enhanced rugosity, maximizing interaction with the cementitious matrix [19]. In this context, previous studies demonstrated that the use of BOFS as fine aggregate [20,21], coarse aggregate [22], or both [23,24] increases the mechanical performance of cementitious materials when compared to traditional materials.

Improvements in strength and durability of cementitious matrices can reduce cement consumption and minimize the need for interventions and repairs. In recent years, the use of nanomaterials to improve the performance of cementitious materials has gained significant attention [25,26]. Numerous studies have investigated cementitious matrices containing carbon black nanoparticles [27,28], carbon nanotubes [29,30], nano-TiO_2 [31,32], and other types of nanomaterials. A particularly noteworthy nanoparticle is nanofibrillated cellulose (NFC), an organic and renewable material that can substantially increase the mechanical strength and durability of cement pastes, mortars, and concretes [33]. These improvements are attributed to several mechanisms. NFCs can serve as nucleation points for hydrated crystals during the early stages of cement hydration [34]. The hydroxyl groups on the fiber surface also interact with hydrated cement products, enhancing the matrix interaction [35]. Notably, the interaction between NFCs and cement grains is stronger than that between cement particles themselves, which, in turn, is greater than the interaction between fibers. [36]. Cao et al. [37] proposed a short-circuit diffusion (SCD) mechanism, where fibers surround the cement particles, forming channels that facilitate water entry and enhance hydration reactions. Lastly, NFCs connect cracks in the matrix through a bridging effect, which prevents crack propagation, enhances matrix strength, and prevents brittle ruptures [38]. Given these mechanisms, different studies have observed the effectiveness of using NFC in cementitious materials to increase mechanical properties [39–44].

For fibers to effectively enhance the performance of cementitious materials, achieving proper dispersion is essential [33,45]. For example, Kong et al. [46] stated that the dispersion of nanofillers is an important factor that affects the mechanical properties for nanocomposites. However, Tian et al. [47] argue that the dispersion of NFC may be challenging due to its agglomeration tendency. According to Zhang et al. [48], the molecular structure of NFC contains a large number of hydroxyl groups, which leads to aggregation and can reduce the reinforcement effects. The dispersion of NFCs can be improved by using surfactants or stabilizing agents, pre-treating fibers (e.g., TEMPO Mediated Oxidation Pretreatment), employing magnetic or mechanical stirring, and utilizing sonication procedures [49]. Sonication, in particular, relies on the principle of cavitation. Ultrasonic waves generated by sonicators induce the formation of bubbles in low-pressure wave regions. The collapse of these bubbles generates a substantial shear force that facilitates the dispersion of fibers [50]. For example, the generated shear stress can reach 100 MPa in typical low viscosity solvents [51]. In this sense, sonication has proven successful in dispersing NFC in several studies [34,45,52,53].

However, previous studies have not explored the production of cementitious composites combining slag aggregates with NFC. Likewise, the optimization of NFC dispersion in eco-efficient cementitious matrices incorporating BOFS has not been investigated. Determining the optimal sonication energy is particularly challenging, mainly because previous research on this topic is scattered and concentrated on conventional cementitious matrices (without incorporation of waste materials). Consequently, potential synergistic effects between BOFS and NFCs in enhancing dispersion mechanisms within cementitious matrices remain unknown.

Motivated by the promising technical benefits provided by BOFS and NFC, this work aimed to clarify the points raised and contribute to the existing literature. To address these knowledge gaps, the present study brings the following contributions: (i) first evaluation of microstructural, rheological, and mechanical properties of mortars containing both BOFS and NFC; (ii) investigation of the relationship between sonication time of NFCs and engineering properties of cementitious composites incorporating BOFS; (iii) combination of different techniques for characterization of the nanosuspensions, including Ultraviolet–visible (UV–vis) spectroscopy, zeta potential analysis, and scanning electron microscopy (SEM); and (iv) combination of different techniques for characterization of the cementitious composites, including tests for determination of workability, compressive strength, flexural strength, eco-efficiency indicators, X-ray diffraction (XRD) and SEM analyses. Consequently, the present work reports the feasibility of producing eco-efficient mortars containing nanomaterials and industrial wastes, providing a more sustainable alternative to traditional materials used in the construction industry.

2. Material and methods

2.1. Material

The conventional binder used to produce the specimens investigated in this research was CPV-ARI cement, corresponding to ASTM type III. This type of cement has a low content of mineral admixtures [54], minimizing interactions between other admixtures and the residues and nanomaterials under investigation. The density of the cement was measured at 3.05 g/cm^3 according to the ABNT NBR 16605 standard [55].

The fine aggregates were BOFS provided by the Arcelormittal company and previously stored for five years in the Laboratory of Civil Construction Materials patio at the Federal University of Ouro Preto (UFOP), State of Minas Gerais, Brazil. Throughout this storage period, the residue underwent a weathering process to stabilize the expansive oxides. Although there are accelerated methods for slag stabilization, such as steam aging and pressurized steam aging, accelerated carbonation, surface treatment, and chemical modification [56–58], weathering is the method that requires the least intervention. The BOFS had a gray color, particle size ranging between 6.35 and 12.5 mm, and a density of 3.57 g/cm^3, as characterized by Martins et al. [59].

A polycarboxylate-based superplasticizer (MC-PowerFlow 4001) was

employed as an admixture to enhance the workability of the composite and decrease the water/cement ratio.

Unbleached NFC from *Pinus*, obtained through a delamination process, was utilized in this study. This material was produced and provided by Embrapa Florestas, situated in Colombo, State of Paraná, Brazil.

2.2. Methods

Fig. 1 presents a flowchart of the methodology adopted in this work, covering the preparation of BOFS aggregates, the evaluation of the impacts of sonication time on the quality of dispersion of NFC solutions, and the production of eco-efficient composites containing BOFS and NFC. The following sections provide a detailed description of each methodology step.

2.2.1. Production of NFCs

Initially, a suspension of non-bleached kraft pulp of loblolly pine (2 % w/v) was prepared using distillate water. Then, it was fragmented using a 450 W blender for 10 min. Subsequently, it was subjected to further grinding using a supermasscolloider Masuko Sangyo Microfluidizer (Masuko Sangyo Ltd., Kawaguchi, Japan). The equipment operated at 1500 rpm, with a distance between discs of 0.1 mm. The cellulose pulp was reloaded 30 times through the friction between the silicon carbide ceramic disks, with the abrasive forces inducing cellulose defibrillation. During this process, the fibers were reduced to nanometric sizes (0.1 and 100 nm). This procedure resulted in a nanosuspension formulation with gel-like characteristics.

Fig. 2 shows a transmission electron microscopy (TEM) image of the material produced by Embrapa Florestas, obtained by Viana et al. [60]. Fibers with diameters smaller than 100 nm can be seen, highlighting the production process's efficiency.

2.2.2. Characterization of NFCs

The solids content of the NFC gel (Fig. 3) was determined by measuring the mass difference between the samples in their natural state and those dried at 100–105 °C for 24 h. The density of the gel was assessed using a 10 ml volumetric flask. Utilizing the values of density and solids content of the gel, as well as the density of water, the density of the nanofibers was calculated. Table 1 presents the main results.

Fourier-transform infrared spectroscopy (FTIR) was also performed using a Nicolet iS50 FTIR Spectrometer (Thermo Scientific) to identify NFC's functional groups and bonds. The analyses were conducted on NFC films at room temperature, with a wavelength ranging from 400 to 4000 cm^{-1} and 128 scans at a resolution of 4 cm^{-1}. The film was

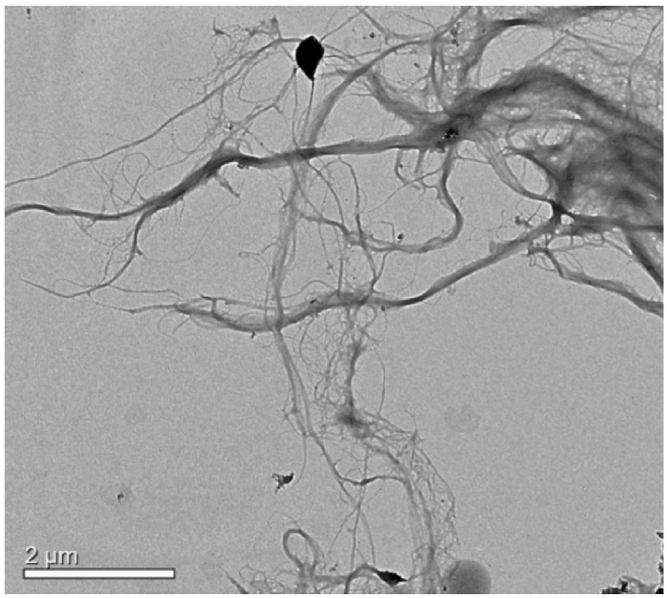

Fig. 2. NFC image obtained by TEM [60].

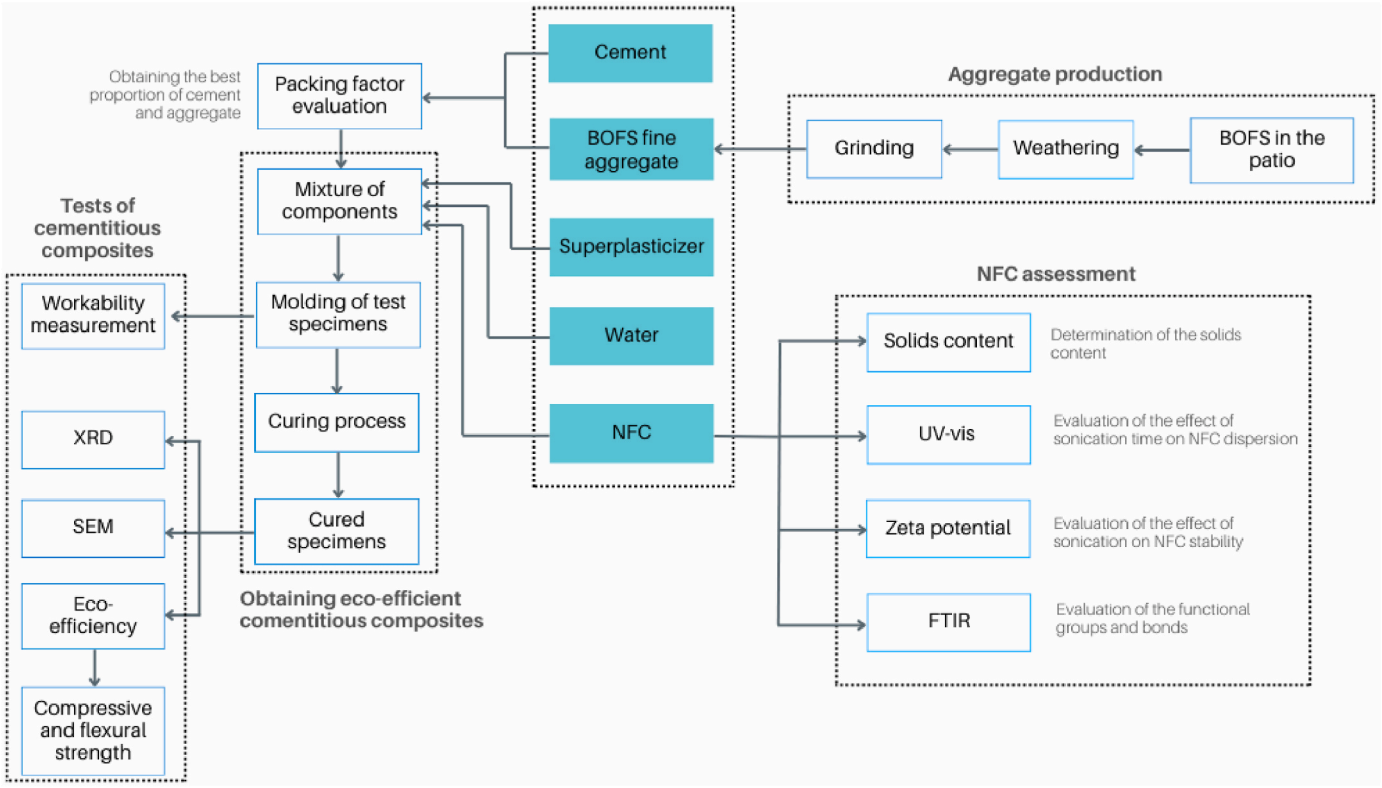

Fig. 1. Flowchart of research methodology.

Fig. 3. NFC gel provided by Embrapa Forestry.

Table 1
Properties of the NFC used in the research.

Property	Result
Gel concentration (%)	1.08
Gel density (g/cm^3)	≅ 1
NFC density (g/cm^3)	1.08

produced from unbleached defibrillated pulp with 1 % solids content. The consistency was adjusted to 0.002 g/ml and homogenized with a magnetic stirrer. The suspension was then poured into a Petri dish and dried in an oven for 24 h at 100 °C.

2.2.3. UV–vis spectroscopy analyses

The Ultraviolet–visible (UV–vis) spectroscopy technique was employed to examine how the sonication time affects the dispersion of NFCs in aqueous solutions. For this purpose, 12.5 ml samples were produced with a concentration of 0.02 % NFC relative to the mass of water. The samples were subjected to different sonication times: 0.00, 0.04, 0.08, 0.16, and 0.32 min/ml of solution. A concentration of 0.02 % NFC was chosen because the spectrophotometer requires more dilute solutions.

Following preparation and sonication, UV–vis analyses were carried out using the FluoroMax Plus fluorometer. The UV–vis lamp was set to a selected wavelength of 300 nm, and absorption measurements were taken within the range of wavelengths from 200 to 800 nm, according to recommendations of Parveen et al. [61,68].

2.2.4. Zeta potential analyses

The zeta potential values of NFC solutions were measured by a Zeta Sizer NanoSeries equipment. Samples were prepared as described in section 2.2.3. Three readings were taken for each sample, and the average value was determined.

2.2.5. Preparation of BOFS aggregates

To obtain the fine aggregates used to produce the cementitious composites, the BOFS (Fig. 4a) was initially dried in an oven for 24 h. Subsequently, the residue was ground in a "Los Angeles" machine (equipment standardized by ABNT NBR 16974 [62]) for 40 min. The particle size distribution curve of the processed material is presented in Fig. 5.

The resulting material was sieved, and the fraction with a diameter smaller than or equal to 2.36 mm was used as BOFS fine aggregates (Fig. 4b).

2.2.6. Packing factor evaluation and production of mortars

The modified Andreassen particle size distribution method [63] was employed to ensure a tightly-packed reference mixture with reliable mechanical properties. The curve was determined with Eq. (1), in which *CPFT* (cumulative percent finer than D) represents the cumulative volume of particles with a size smaller than a diameter D, D_L is the diameter of the largest particle, D_S is the diameter of the smallest particle, and q is the distribution coefficient.

$$CPFT(\%) = 100\frac{D^q - D_S^q}{D_L^q - D_S^q} \quad (1)$$

Distribution coefficient q, as reported in the literature, ranges from 0.21 to 0.37, with values between 0.25 and 0.30 being applied for high-performance and conventional concrete [64]. In this study, a q value of 0.25 was chosen. Additionally, a D_L of 2.36 mm (representing the largest diameter of the fine slag aggregate produced) and a D_S of 0.0001 mm were used in this research. The modified Andreassen curve determined that the optimal mixture consisted of 20 % cement and 80 % BOFS sand, following a 1:4 vol ratio. Fig. 6 shows the curve corresponding to the

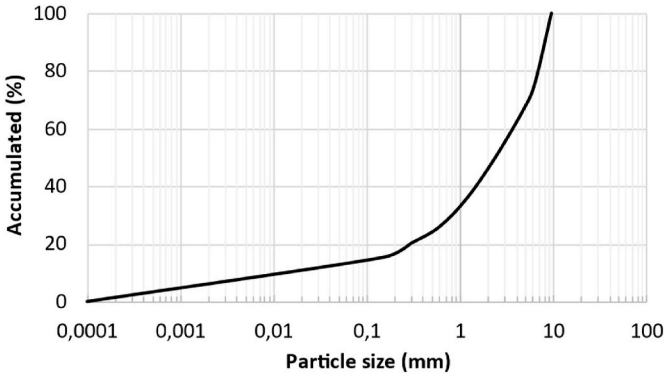

Fig. 5. Particle size curve of the BOFS aggregate produced with 40 min of grinding.

Fig. 4. BOFS: (a) before grinding; (b) after grinding and sieving.

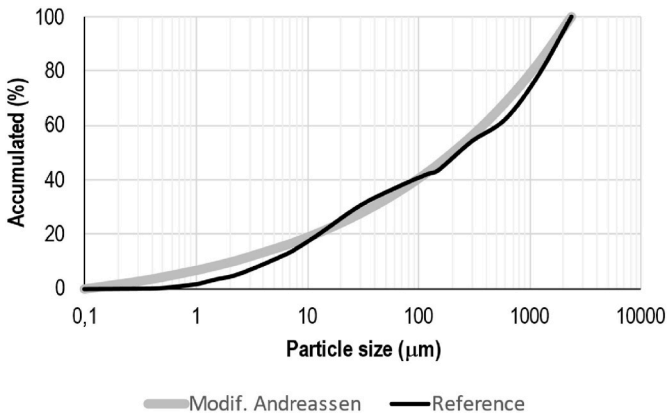

Fig. 6. Particle size distribution of the mixture 1:4 and modified Andreassen curve for $D_L = 2360$ μm, $D_S = 0.1$ μm and $q = 0.25$.

reference mixture.

2.2.7. Preparation of the cementitious composites

To assess the impact of fiber dispersion, cementitious composites were produced with a cement-to-aggregate ratio of 1:4 (by volume) and an NFC content of 0.1 % (by weight of cement). The fiber concentration adopted was based on the work of Kamasamudram et al. [65], which used unbleached NFC and verified an increase in flexural strength. Superplasticizer (SP) was used to enhance the workability of the mixtures, with a content of 2.80 % (by weight of cement). The ratio between the volume of dry material and the final volume of the mixture was 0.72, resulting in a water-to-cement ratio of approximately 0.63.

The procedures used to produce the specimens are represented in Fig. 7. In the initial phase, an aqueous NFC solution was prepared. The specified amounts of water and NFC were subjected to different sonication durations: 0, 0.04, 0.16, and 0.32 min/ml of solution, using a 50 W, 20 kHz probe sonicator. The sonication times were chosen for practical reasons, with 0.32 min/ml (approximately 30 min of sonication for full volume) as the maximum to avoid slowing down specimen production. The intermediate sonication times were selected to cover different sonication levels used in previous literature [45,66,67]. Dry BOFS sand and cement were mixed. Subsequently, the superplasticizer and the sand-cement blend were added to the NFC solution and mechanically mixed for 10 min, followed by an additional 5 min of stirring to complete the mixture. The resulting mixture was poured into acrylic molds measuring 2 cm × 2 cm × 8 cm, in two layers. Each layer was compacted on a vibrating table for 15 s. After molding, the specimens were cured inside a moist room (23 ± 2 °C and 95 % humidity). Additionally, cylindrical specimens measuring 3 cm in diameter and 6 cm in height were molded for microstructural evaluation.

2.2.8. Workability tests

Before molding the specimens, the mixture's workability was assessed using a mini-cone-slump test. A Kantro cone mold, with dimensions of 57 mm in height, 19 mm at the top diameter, and 38 mm at the bottom diameter [68], was used for the test. Three layers of the mixture were added to the Kantro cone mold, with the first layer compacted with 15 strokes, the second layer with ten strokes, and the third layer with five strokes, aimed at removing air bubbles. Subsequently, the Kantro cone mold was lifted carefully, and ten drops from the flow table were applied. Finally, three values of spreading diameters were measured, and the average was calculated as the spreading diameter.

2.2.9. Microstructural analyses

After a curing period of 28 days, small slices of the intermediate portion of the cylindrical specimens were extracted for microstructural analyses. The hydration process was then interrupted with isopropyl alcohol, according to the methodology described by Scrivener et al. [69]. This material was subsequently utilized in various microstructural studies.

X-ray diffraction (XRD) analysis was conducted using a D8Discover

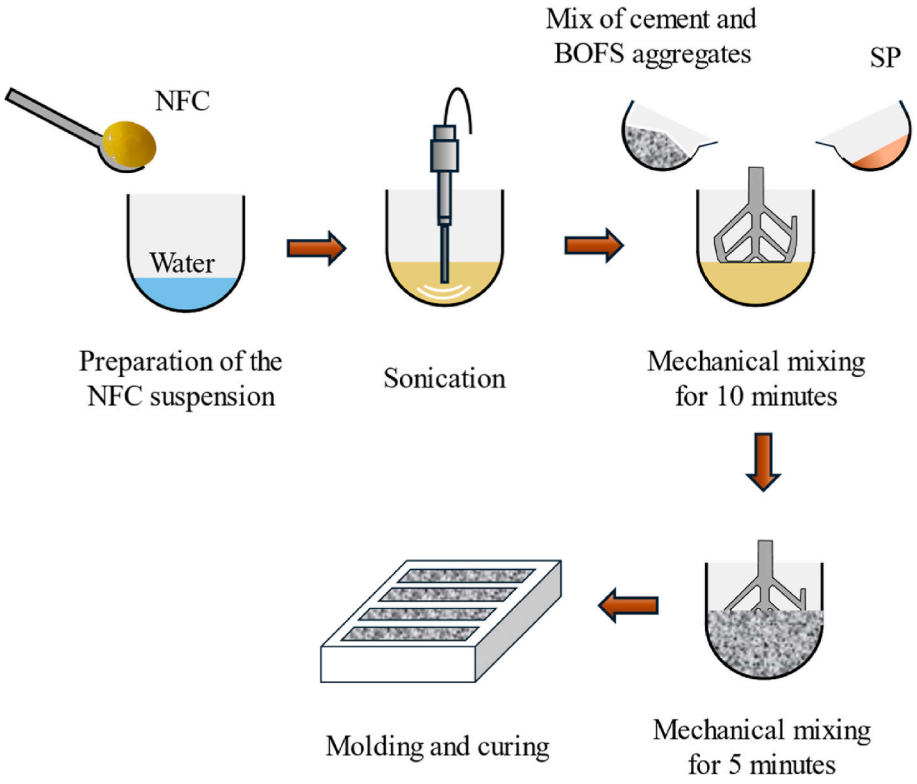

Fig. 7. Preparation of the cementitious composites.

diffractometer in the Department of Physics at the Federal University of Viçosa (UFV). The radiation source employed was CuKα, with a wavelength (λ) of 1.5418 Å, scanning range (2θ) from 10° to 80°, 0.05° step-size and an accumulated time per step of 1 s.

Scanning electron microscopy (SEM) images of NFC solutions with sonication times of 0, 0.04, 0.08, 0.016, and 0.32 min/ml were captured using a JEOL JSM-6010LA microscope at 15 kV, located in the Department of Physics (UFV). SEM images of cementitious composites were captured at the Center for Microscopy and Microanalysis (UFV), utilizing a Leo 1430 VP Scanning Electron Microscope operating at 15 kV.

2.2.10. Mechanical and eco-efficiency properties

The cementitious composites were subjected to compression and flexural tests after a curing period of 28 days [70–72]. Additionally, the eco-efficiency of the mixtures was determined following the methodology of Damineli et al. [73,74]. Eco-efficiency was defined by two parameters: cement intensity for compressive strength - CI_c (Eq. (2)), and cement intensity for flexural strength - CI_f (Eq. (3)). In these equations, b is the amount of binder (Portland cement), p_c is the performance achieved (compressive strength) and p_f is the flexural strength.

$$CI_c = \frac{b}{p_c} \tag{2}$$

$$CI_f = \frac{b}{p_f} \tag{3}$$

Lower values of CI_c and CI_f indicate higher eco-efficiency. Specifically, these parameters represent the amount of cement required to reach 1 MPa of compressive and flexural strength after a curing time of 28 days, respectively.

3. Results and discussion

3.1. FTIR

Fig. 8 illustrates the FTIR spectrum of the NFC film. The spectrum reveals the typical peaks of cellulose, such as bands at 895 cm^{-1} (β-glycosidic bonds between glucose units), 1027 cm^{-1} (C–*O*–C bonding of asymmetric 1,4-glycosidic bonds of D-glucose), 1160 cm^{-1} (angular deformation of C–O bonds of alcohols), 1428 cm^{-1} (asymmetric deformation of CH and CH_2 groups), 1636 cm^{-1} (carboxylic acid bonds), 2890 cm^{-1} (C–H bonds) and 3328 cm^{-1} (stretching and vibration of the O–H bond on the surface of the fibers) [75].

The presence of O–H groups on the NFC surface is advantageous since they bind through hydrogen bonds to C–S–H and calcium hydroxide in the cement matrix, in addition to intensifying the hydration process of the cement particles [35,42,44,76]. Thus, the fibers contribute to a better mechanical performance of the composites.

3.2. UV–vis

UV–vis spectroscopy analyses provide the absorption of light by samples as a function of wavelength. As light passes through the sample, it interacts with the material, causing electronic transitions. This interaction is described by the Beer-Lambert law, which relates the incident light intensity (I_0) and the light intensity measured after interaction with the material (I) [77]. A higher concentration of particles in solution leads to greater light interaction, making UV–vis a suitable technique for measuring nanocellulose dispersion.

Fig. 9 illustrates absorbance curves for various sonication times of aqueous NFC solutions. The unsonicated sample displayed the lowest absorbance values, while increased sonication time correlated with higher absorbance values up to 0.16 min/ml. However, longer sonication times resulted in a absorbance decrease. These results align with those obtained by Parveen et al. [61,68] for microcrystalline cellulose solutions prepared under different sonication times. For a short sonication time, these authors observed that larger cellulose agglomerates tended to sediment, causing lower absorbance values. Up to 30 min of dispersion, sonication efficiently reduced the size of the agglomerates, with a consequent decrease in sedimentation and higher absorbance values. However, longer times promoted reagglomeration of the cellulose, reducing the absorbance of the samples. Therefore, the unbleached NFC evaluated in this work appears to behave similarly to the material evaluated by Parveen et al. [61,68]. Carbon nanotubes (CNT), nanomaterials that also have a high length/area ratio, exhibited the same behavior under increasing sonication duration, with improved dispersion up to intermediate sonication times and reagglomeration at longer times due to increases in energy and temperature [78].

SEM images also helped to explain the results obtained in this work. In samples that were not sonicated, a specific agglomeration of fibers were observed in some regions (Fig. 10a). This suggests inadequate distribution of NFCs, potentially hindering the enhancement of mechanical properties in the cementitious composites. When not dispersed, the fibers sediment, creating regions with a higher material concentration. According to Mejdoub et al. [34] and Sun et al. [44], in higher concentrations, NFCs agglomerate, forming fiber networks. After the

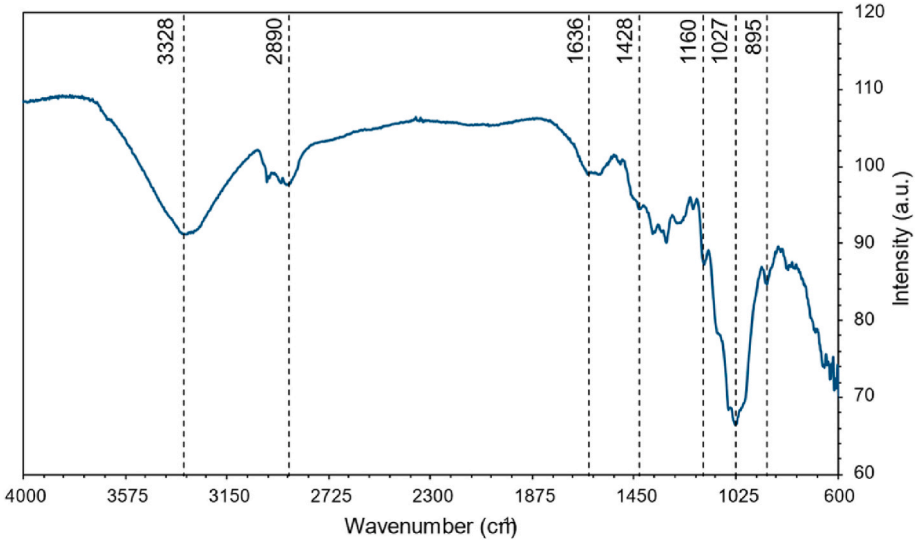

Fig. 8. FTIR spectra of the NFC film.

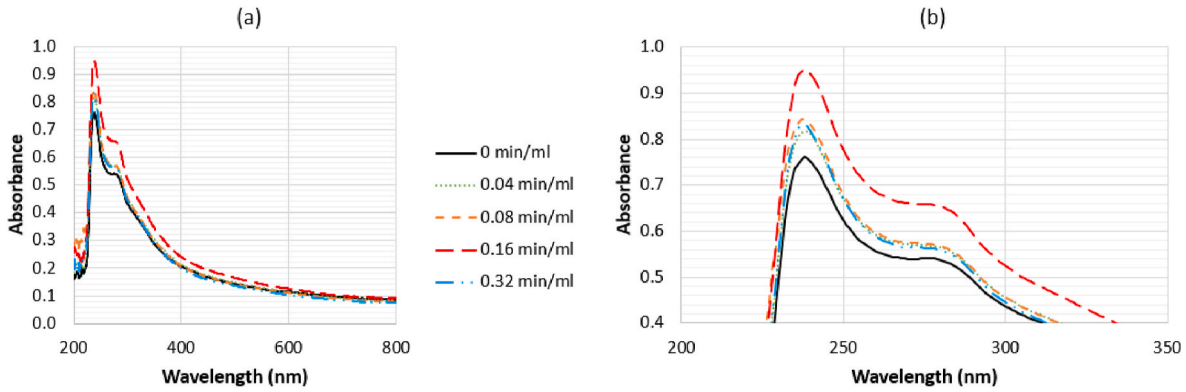

Fig. 9. Absorbance of solutions with different sonication times. (a) Overall UV–vis spectra; (b) detailed view of the initial portion of the UV–vis spectra.

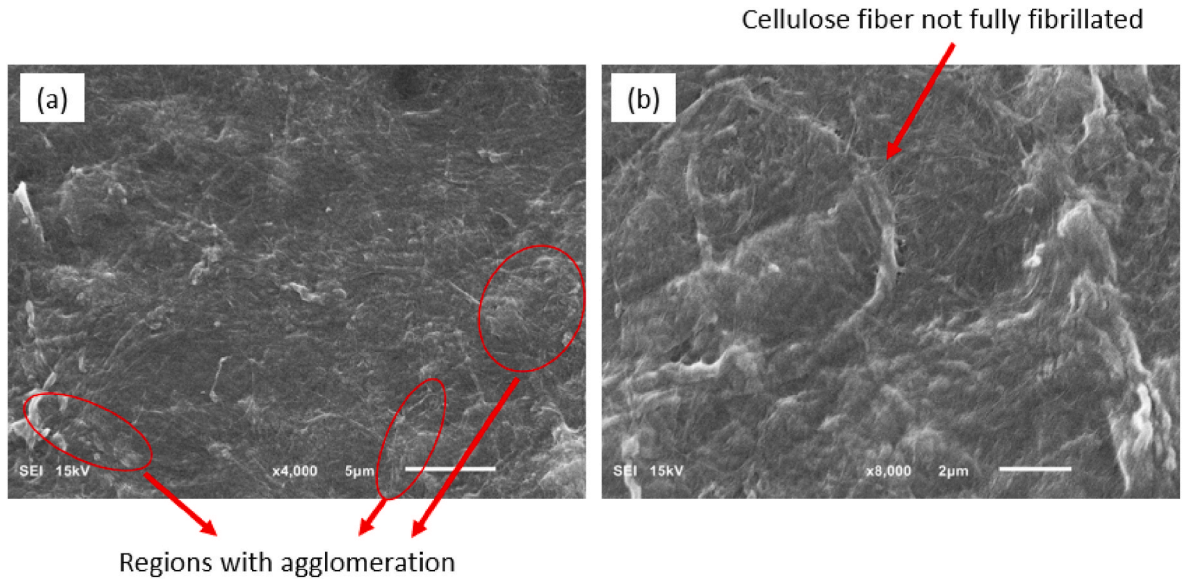

Fig. 10. NFC samples without sonication: (a) 4000x magnification, (b) 8000× magnification.

curing process, these NFC agglomerates create pores within the cement matrix, i.e., weak zones where stresses are concentrated. This concentration of stresses induces the formation and propagation of cracks, which can culminate in the failure of the cementitious composite. Moreover, Fig. 10b highlights one fiber that is not fully fibrillated, indicating a potential area for optimization in the NFCs production process.

In Fig. 11, longer fibers with improved individualization are clearly evident, indicating more efficient dispersion resulting from sonication processes. The high shear stresses generated by sonication procedures can dismount the fiber networks, separate them, and improve dispersion. In this way, weak zones and points of stress accumulation are reduced, preventing the formation of cracks. In addition, an improvement in the distribution of NFCs maximizes the interaction of the fibers with the matrix, allowing them to act through a bridging effect and preventing the proliferation of cracks during the loading of the cementitious composite.

3.3. Zeta potential

The colloidal stability of cellulose nanomaterials is typically maintained through the electrostatic repulsion of charged groups on their surface. The zeta potential technique, which measures the surface charge density of suspended particles, is commonly employed to assess the stability of suspensions [79].

Fig. 12 displays the zeta potential values for samples subjected to different sonication times. In the absence of sonication, the samples exhibited the least negative charge (−28.3 mV) with a broad dispersion of values. Upon sonication, the charge becomes progressively more negative, reaching −39.1 mV at 0.08 min/ml and stabilizing around −37 mV. Higher zeta potential values indicate improved stability of the nanofibers, with suspensions between ±10 and ± 30 mV being considered slightly unstable and between ±30 and ± 40 mV being moderately stable [66]. Therefore, sonication emerges as an effective method for enhancing the suspension stability of unbleached NFC, in agreement with what was observed in the SEM images. In association with sonication, other dispersion techniques (e.g., use of surfactants, stabilizing agents, fiber pretreatment methods like TEMPO-mediated oxidation [49], etc.) could be explored to further enhance the stability and performance of NFC suspensions.

3.4. Workability

The spreading diameters of the different mortars produced in this research are shown in Fig. 13. The sample without sonicated NFCs exhibited the largest spreading diameters. In contrast, the other treatments resulted in smaller spreading diameters. This difference can be attributed to the hydrophilic nature of the nanofibers [45]. Improved fiber dispersion increases the surface area of NFCs, enhancing water retention and consequently reducing water availability in the system. As

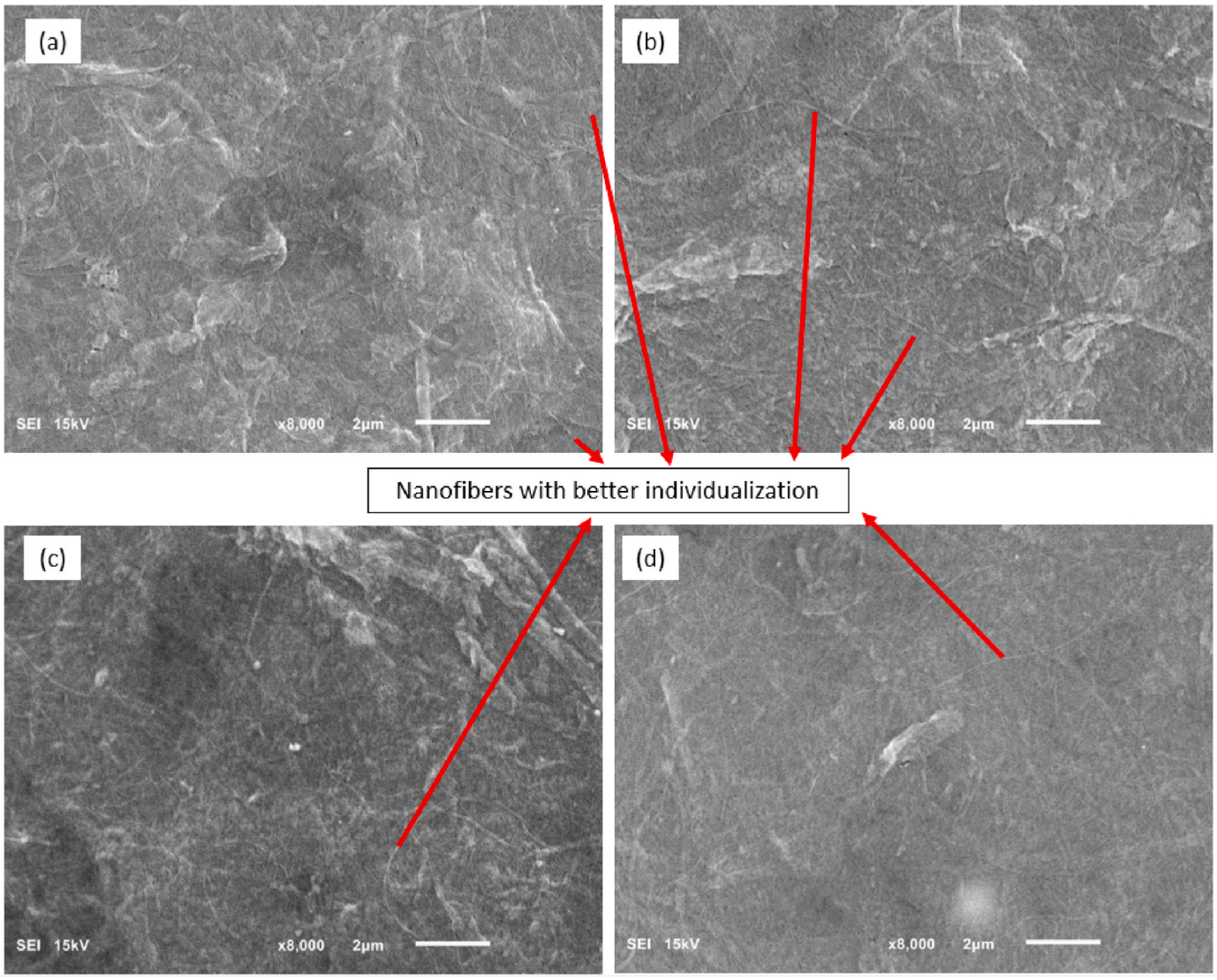

Fig. 11. NFC samples with time sonication of (a) 0.04 min/ml, (b) 0.08 min/ml, (c) 0.16 min/ml and (d) 0.32 min/ml, at a 8000x magnification.

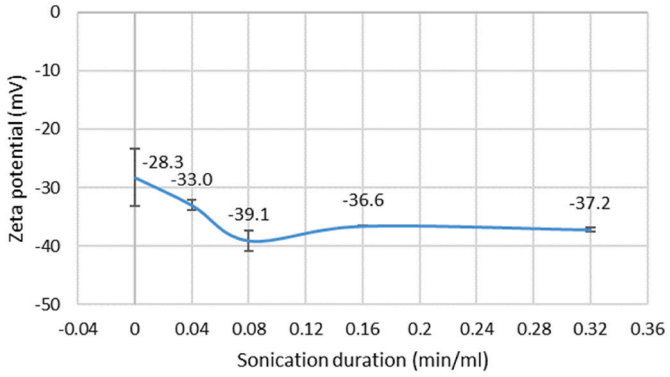

Fig. 12. Variation of zeta potential values as a function of sonication duration.

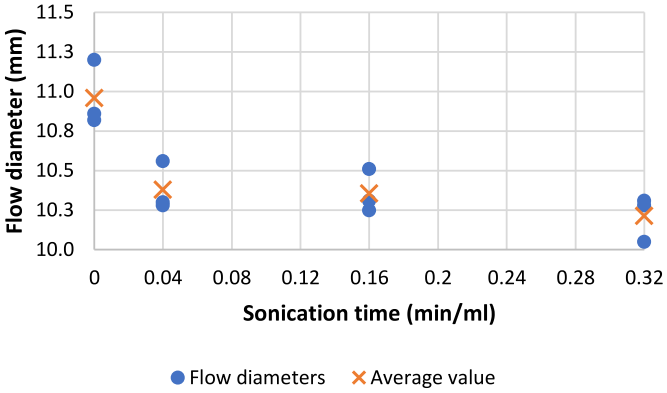

Fig. 13. Spreading diameters of samples as a function of sonication time.

a result, the workability of the samples decreases. These findings align with the UV–vis results and SEM images, indicating that sonication promotes more effective fiber dispersion.

To achieve higher amounts of added NFCs or improved fiber dispersion, it is advisable to adjust the superplasticizer dosage carefully. This adjustment would prevent adverse effects on the compaction and molding processes of the test specimens [33].

3.5. Mechanical performance

The results presented in Fig. 14 and Table 2 indicated that the distinct sonication treatments did not affected significantly the

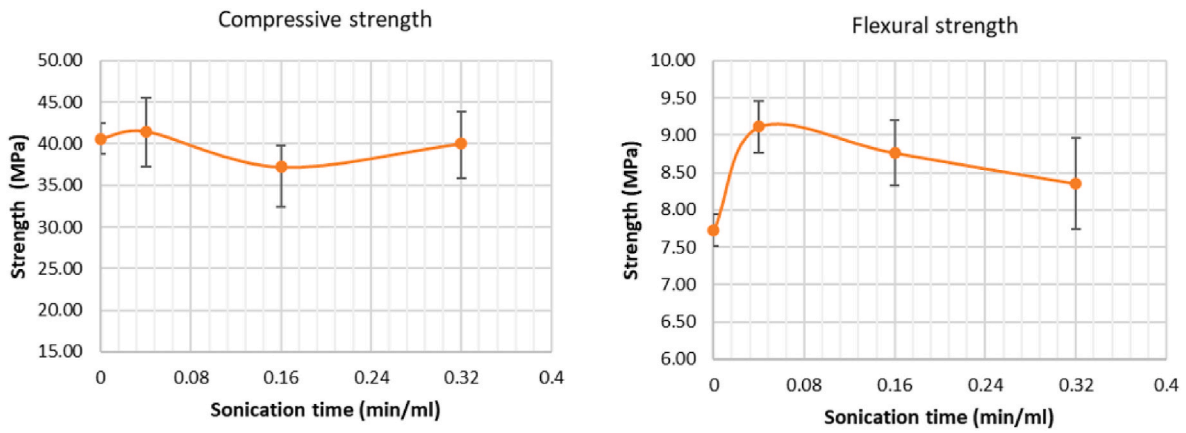

Fig. 14. Compressive and flexural strength of specimens subjected to different sonication times.

Table 2
Tukey test ($\alpha = 5$ %) for the compressive strength of mixtures at 28 days.

Sonication time (min/ml)	N	Mean (MPa)	Grouping
0.04	8	41.42	A
0	7	40.616	A
0.32	8	40.00	A
0.16	8	37.22	A

compressive strength of the specimens. In other words, longer sonication times do not necessarily lead to greater compressive strength. However, the results indicated that longer sonication times can contribute to significant improvements in flexural strength. There is an increase of 17.9 % and 13.4 % for sonication times of 0.04 min/ml and 0.16 min/ml, respectively (Fig. 14 and Table 3). These results align with those obtained from the UV–vis, potential zeta, and SEM techniques, in which fiber dispersion and stability are less effective without sonication. With a sonication time of 0.32 min/ml, the strength gain compared to the reference is lower (8.1 %). Although the flexural strengths are statistically equal between the sonicated samples, a tendency towards optimum strength is observed for intermediate sonication times.

The UV–vis technique was able to effectively differentiate the non-sonicated sample from the sonicated ones. Among the sonicated samples, the one treated for 0.16 min/ml exhibits higher absorbance than the others, suggesting superior dispersion relative to the rest. In the other techniques used in the present research, this sonication time did not provide the best dispersion results. Therefore, a more in-depth investigation into the application of this technique in evaluating the dispersion of NFCs is recommended to enhance its reliability in correlating sonication time, fiber dispersion, and absorbance results.

Within the cementitious matrix, NFCs contribute to mechanical strength through various mechanisms: acting as nucleation points, supplying water to cement particles, and contributing to a bridging effect that prevents crack propagation. [37,80]. In the specimens evaluated in this work, the most influential mechanism was the bridging effect, leading to notable improvements in flexural strength. This conclusion is supported by XRD results, where curves for different sonication times exhibit similarity (Fig. 15), suggesting no significant variations in mineralogical composition that justify increased strength with improved sonication.

Table 3
Tukey test ($\alpha = 5$ %) for the flexural strength of mixtures at 28 days.

Sonication time (min/ml)	N	Mean (MPa)	Grouping	
0.04	4	9.115	A	
0.16	4	8.766	A	
0.32	4	8.355	A	B
0	3	7.729		B

Furthermore, the SEM images presented in Fig. 16 reinforce these findings. Samples without sonication exhibit suboptimal fiber distribution (Fig. 16a) with noticeable agglomeration points (Fig. 16b). In contrast, samples with higher flexural strength display improved fiber distribution (Fig. 17a) and the presence of fibers contributing to the bridging effect (Fig. 17b). Therefore, it can be inferred that sonication enhances the distribution of fibers into the matrix, optimizing the bridging effect.

Fig. 15 shows the XRD spectra of the samples. The black letters indicate compounds originating from cement and the red letters compounds associated with the presence of slag. XRD signatures of portlandite [$Ca(OH)_2$] were identified, derived from the hydration of alite (C_3S) and belite (C_2S) of cement particles. The presence of C_3S and C_2S signatures in the samples indicates that the hydration of Portland cement grains was incomplete. The hydration of C_2S and C_3S compounds of slag is much slower than that of cement, with a fraction of these minerals being found unhydrated after 90 days of curing [81]. Since the slag aggregates were ground for the preparation of the XRD samples of this study, the C_2S inside BOFS aggregates were identified in the diffractograms. This result agrees with the findings of Franco de Carvalho et al. [82], who discussed the XRD patterns of the same BOFS used in this work.

Some portlandite crystals and structures of calcite ($CaCO_3$) can be also attributed to the weathering and aging process that the residue has undergone. During this process, lime (CaO) stabilizes and transforms into portlandite and calcite [83]. CaO was identified in the XDR spectra, which indicates that even an extended weathering period was insufficient to eliminate the existing lime. The minerals brownmilerite (C_4AF) and wuestite observed in the XDR patterns also come from the slag used in this study [59,82].

3.6. Eco-efficiency of composites

Table 4 shows the eco-efficiency indices obtained for the different mixtures. The results indicated that the sonication time has a minimal impact on the cement intensity for compressive strength (CI_c). In this case, the obtained values range between 10.8 and 11.8 (kg/m^3)/MPa, falling into the category of conventional concrete, where mixtures typically exhibit a cement intensity greater than 10 (kg/m^3)/MPa [84].

In contrast, the application of sonication procedures effectively reduces the cement intensity for flexural strength (CI_f). Compared to the reference specimen, the sonication time of 0.04 min/ml decreases the CI_f by 15.2 %, and the sonication time of 0.16 min/ml decreases the CI_f by 11.8 %. This implies that with sonication, achieving each additional 1 MPa in flexural strength demands less cement, thereby enhancing the eco-efficiency of the composites. Therefore, ensuring the proper

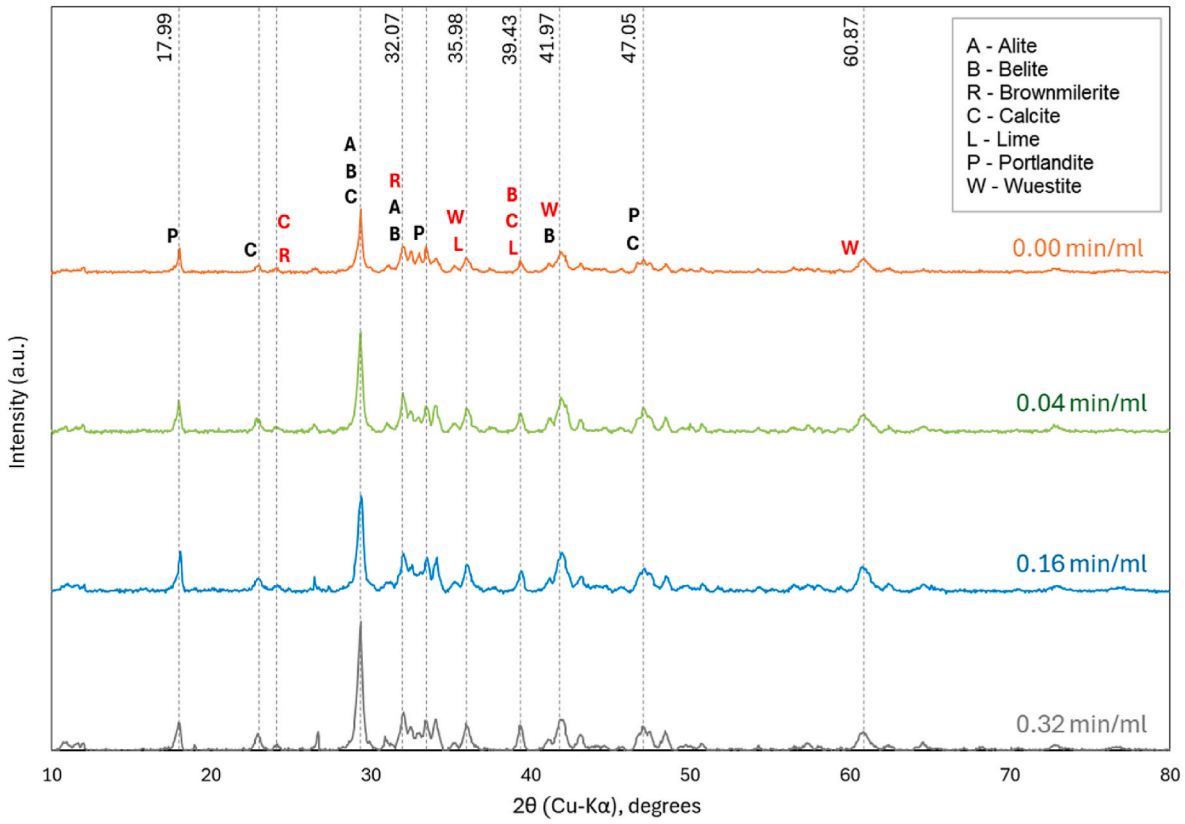

Fig. 15. Results of XRD analysis of cementitious composites with different sonication times.

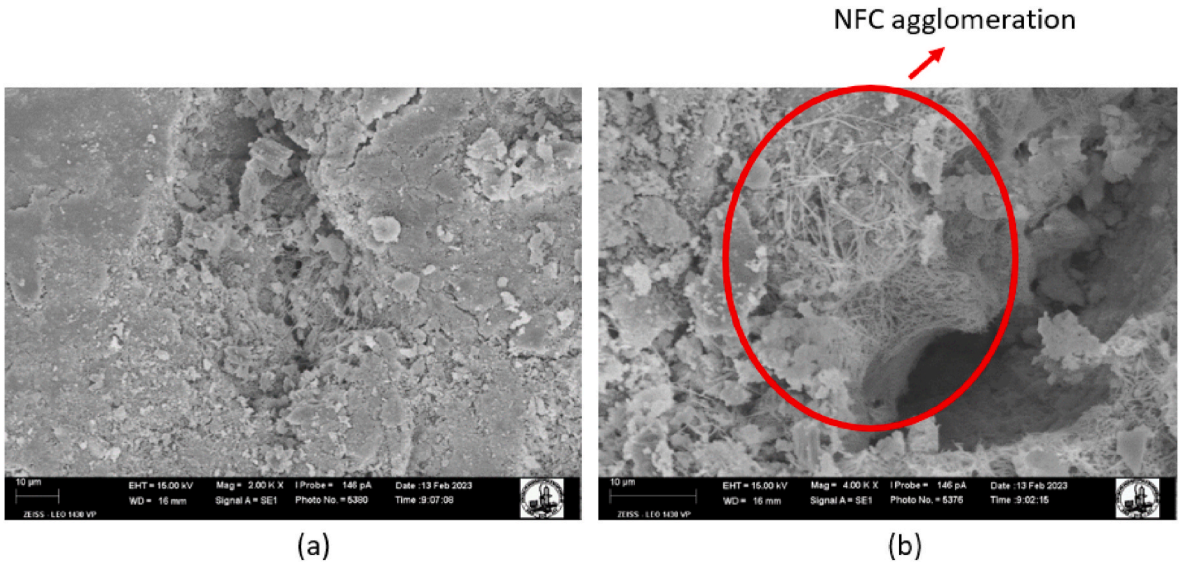

Fig. 16. SEM images of the cement matrix with NFC without sonication: (a) 2000x magnification, (b) 4000× magnification.

dispersion of cellulose fibers improves the flexural properties of the composites and their eco-efficiency, allowing for reduced cement consumption to achieve a targeted performance.

The cement consumption of the composites was 438.4 kg/m^3. By using BOFS as a replacement for natural aggregates, a waste consumption of 1997.6 kg/m^3 of concrete was achieved. In terms of dry material volume, 80 % of the cementitious composite is waste, demonstrating that the mortar designed in this research presents a high rate of waste incorporation. Expanding cement products with a high volume of BOFS incorporation can increase the demand for this residue, leading to its valorization and consequently reducing its inappropriate disposal in landfills. In addition, it would reduce the demand for extraction of natural aggregates, mitigating related environmental impacts.

Evaluating all the UV–vis, SEM, zeta potential, and eco-efficiency results, it is noted that sonication times of 0.04 min/ml and 0.016 min/ml yield the most effective dispersions of nanomaterials and, consequently, mortars with higher mechanical strength. Considering the association of sonication time with sample volume, a recommendation for large-scale production of these cementitious materials would be a sonication time of 0.04 min/ml. This choice would significantly reduce

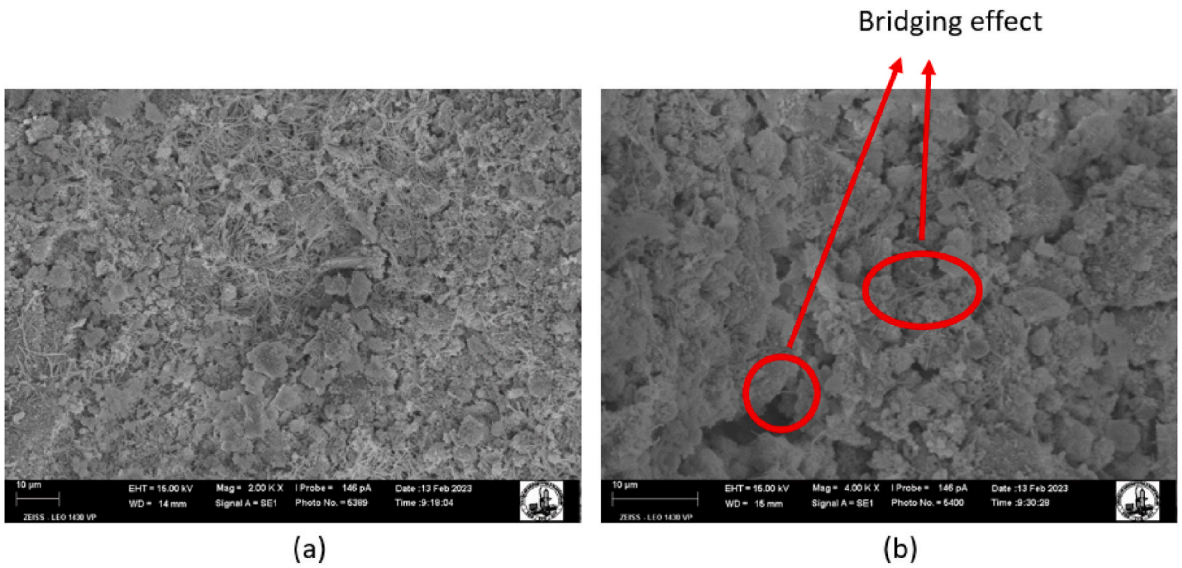

Fig. 17. SEM images of the cement matrix with NFC sonicated for 0.04 min/ml: (a) 2000x magnification, (b) 4000× magnification.

Table 4
Consumption of materials and eco-efficiency of mixtures.

Sonication time (min/ml)	CI_c [(kg/m^3)/MPa]	CI_f [(kg/m^3)/MPa]
0	10.8	56.7
0.04	10.6	48.1
0.16	11.8	50.0
0.32	11.0	52.5

* CI_c: cement intensity for compressive strength; CI_f: cement intensity for flexural strength.

both the time required for composite production and energy consumption.

4. Conclusions and future perspectives

This study reported the impact of sonication time on NFC dispersion and the eco-efficiency of nanomodified cementitious composites with steel slag aggregate, yielding key conclusions on the optimal dispersion process and the resulting improvements in the material's performance, as follows.

1. The UV–vis results revealed that sonication promotes more homogeneous solutions with smaller aggregates, which sediment less. Therefore, it can be inferred that sonication effectively enhanced the dispersion of NFCs.
2. The sonication of NFC solutions also increased their zeta potential. Sonicated samples exhibited zeta potentials ranging from −33.0 to −39.1 mV, indicating moderate stability.
3. For fresh cementitious, sonication of NFCs decreases the workability, i.e., improved fiber dispersion results in a larger surface area, leading to increased water retention.
4. Sonication time had a positive impact on the flexural strength of the specimens. Mortars subjected to sonication times of 0.04 and 0.16 min/ml showcased strength gains of 17.9 % and 13.4 % compared to the reference specimen. These results, in association with SEM images, suggest that improved fiber dispersion favors the bridging effect in cementitious composites containing BOFS and NFCs.
5. Additionally, the enhanced dispersion of fibers through sonication procedures contributes to a reduction in the cement intensity index CI_f and, consequently, increases the eco-efficiency of the cementitious materials. Therefore, sonication was efficient in producing composites containing NFC and BOFS, a result not demonstrated in previous works.
6. Finally, UV–vis, SEM, zeta potential, and eco-efficiency results reveal that the sonication time of 0.04 min/ml is promising for large-scale production of the cementitious composites evaluated in this work. This choice represents less time and energy for production combined with good mechanical performance and eco-efficiency of the composites.

To optimize the fibers-dispersion level and enhance the eco-efficiency of cementitious composites containing BOFS and NFC, the following suggestions are proposed.

1. Extending the investigation into the influence of sonication procedures on the dispersion of different fiber contents. It is advisable to explore how the NFC concentration in the solution might affect the sonication time to achieve improved dispersion and to use a Scanning Electron Microscope with Field Emission Gun (SEM-FEG) and TEM to reinforce the morphological analysis of the dispersions.
2. Assessing the effectiveness of incorporating different types of surfactants and stabilizers into NFC suspensions and examine their impact on the eco-efficiency and mechanical strength of the resulting cement-based materials.
3. Investigating the simultaneous application of sonication, surfactants, and/or stabilizers to ascertain potential synergistic effects between them. This exploration can provide insights into the most suitable methodology for achieving optimal NFC dispersion.

Funding

This research was financed, in part, by the Coordenação de Aperfeiçoamento de Pessoal de Nível Superior (CAPES) - Brazil - finance code 001, and by the Brazilian agencies FAPEMIG and CNPq.

Declaration of competing interest

The authors declare that they have no known competing financial interests or personal relationships that could have appeared to influence the work reported in this paper.

Acknowledgments

This study was financed in part by the Coordenação de

Aperfeiçoamento de Pessoal de Nível Superior – Brasil (CAPES) – Finance Code 001. The authors would like to thank the Department Civil Engineering Department (UFV), the research group on Sustainable and Innovative Construction (SICon – https://www.sicon.ufv.br/en/), the Brazilian Agricultural Research Corporation – Forestry (Embrapa Forestry) and Gabriel Tomaz Massardi which supported the present research.

References

[1] Sev A. How can the construction industry contribute to sustainable development? A conceptual framework. Sustain Dev 2009;17:161–73. https://doi.org/10.1002/sd.373.
[2] Li X, Qin D, Hu Y, Ahmad W, Ahmad A, Aslam F, et al. A systematic review of waste materials in cement-based composites for construction applications. J Build Eng 2022;45:103447. https://doi.org/10.1016/j.jobe.2021.103447.
[3] Cantero B, Sáez del Bosque IF, Sánchez de Rojas MI, Matías A, Medina C. Durability of concretes bearing construction and demolition waste as cement and coarse aggregate substitutes. Cem Concr Compos 2022;134. https://doi.org/10.1016/j.cemconcomp.2022.104722.
[4] Wu H, Xiao J, Liang C, Ma Z. Properties of cementitious materials with recycled aggregate and powder both from clay brick waste. Buildings 2021;11. https://doi.org/10.3390/buildings11030119.
[5] Abera Y, Shanko A. Performance of concrete materials containing recycled aggregate from construction and demolition waste. Results Mater 2022;14:100278. https://doi.org/10.1016/j.rinma.2022.100278.
[6] González JS, Boadella IL, Gayarre FL, Pérez CLC, López MS, Stochino F. Use of mining waste to produce ultra-high-performance fibre-reinforced concrete. Materials 2020;13:1–13. https://doi.org/10.3390/ma13112457.
[7] Benahsina A, El Haloui Y, Taha Y, Elomari M, Bennouna MA. Natural sand substitution by copper mine waste rocks for concrete manufacturing. J Build Eng 2022;47:103817. https://doi.org/10.1016/j.jobe.2021.103817.
[8] El Machi A, Mabroum S, Taha Y, Tagnit-Hamou A, Benzaazoua M, Hakkou R. Use of flint from phosphate mine waste rocks as an alternative aggregates for concrete. Constr Build Mater 2021;271:121886. https://doi.org/10.1016/j.conbuildmat.2020.121886.
[9] Liu H, Li Q, Ni S. Assessment of the engineering properties of biomass recycled aggregate concrete developed from coconut shells. Constr Build Mater 2022;342:128015. https://doi.org/10.1016/j.conbuildmat.2022.128015.
[10] Shao K, Du Y, Zhou F. Feasibility of using treated corn cob aggregates in cement mortars. Constr Build Mater 2021;271:121575. https://doi.org/10.1016/j.conbuildmat.2020.121575.
[11] Khankhaje E, Salim MR, Mirza J, Hussin MW, Rafieizonooz M. Properties of sustainable lightweight pervious concrete containing oil palm kernel shell as coarse aggregate. Constr Build Mater 2016;126:1054–65. https://doi.org/10.1016/j.conbuildmat.2016.09.010.
[12] Mirnezami SM, Hassani A, Bayat A. Evaluation of the effect of metallurgical aggregates (steel and copper slag) on the thermal conductivity and mechanical properties of concrete in jointed plain concrete pavements (JPCP). Constr Build Mater 2023;367:129532. https://doi.org/10.1016/j.conbuildmat.2022.129532.
[13] Franco de Carvalho JM, Fontes WC, Azevedo CF de, Brigolini GJ, Schmidt W, Peixoto RAF. Enhancing the eco-efficiency of concrete using engineered recycled mineral admixtures and recycled aggregates. J Clean Prod 2020;257. https://doi.org/10.1016/j.jclepro.2020.120530.
[14] Franco de Carvalho JM, Melo TV de, Fontes WC, Batista Jo dos S, Brigolini GJ, Peixoto RAF. More eco-efficient concrete: an approach on optimization in the production and use of waste-based supplementary cementing materials. Constr Build Mater 2019;206:397–409. https://doi.org/10.1016/j.conbuildmat.2019.02.054.
[15] Fernández-González D, Prazuch J, Ruiz-Bustinza I, González-Gasca C, Piñuela-Noval J, Verdeja LF. The treatment of Basic Oxygen Furnace (BOF) slag with concentrated solar energy. Sol Energy 2019;180:372–82. https://doi.org/10.1016/j.solener.2019.01.055.
[16] Worldsteel Association. 2021 World steel in figures. 2021.
[17] Yildirim IZ, Prezzi M. Chemical, mineralogical, and morphological properties of steel slag. Adv Civ Eng 2011;2011. https://doi.org/10.1155/2011/463638.
[18] Geiseler J. Use of steelworks slag in Europe. Waste Manag 1996;16:59–63. https://doi.org/10.1016/S0956-053X(96)00070-0.
[19] Qasrawi H. The use of steel slag aggregate to enhance the mechanical properties of recycled aggregate concrete and retain the environment. Constr Build Mater 2014;54:298–304. https://doi.org/10.1016/j.conbuildmat.2013.12.063.
[20] Guo Y, Xie J, Zheng W, Li J. Effects of steel slag as fine aggregate on static and impact behaviours of concrete. Constr Build Mater 2018;192:194–201. https://doi.org/10.1016/j.conbuildmat.2018.10.129.
[21] Guo Y, Xie J, Zhao J, Zuo K. Utilization of unprocessed steel slag as fine aggregate in normal- and high-strength concrete. Constr Build Mater 2019;204:41–9. https://doi.org/10.1016/j.conbuildmat.2019.01.178.
[22] Wang GC. Slag use as an aggregate in concrete and cement-based materials. https://doi.org/10.1016/b978-0-08-100381-7.00011-2; 2016.
[23] Stief JN de P, Maia N da S, Peixoto RAF. Determinação experimental do módulo de elasticidade do concreto convencional e com agregados de escória de aciaria. Educ Tecnol 2009;14:22–7.
[24] Aparicio S, Hernández MG, Anaya JJ. Influence of environmental conditions on concrete manufactured with recycled and steel slag aggregates at early ages and long term. Constr Build Mater 2020;249:118739. https://doi.org/10.1016/j.conbuildmat.2020.118739.
[25] Yoo DY, Oh T, Banthia N. Nanomaterials in ultra-high-performance concrete (UHPC) – a review. Cem Concr Compos 2022;134:104730. https://doi.org/10.1016/j.cemconcomp.2022.104730.
[26] Onaizi AM, Huseien GF, Lim NHAS, Amran M, Samadi M. Effect of nanomaterials inclusion on sustainability of cement-based concretes: a comprehensive review. Constr Build Mater 2021;306:124850. https://doi.org/10.1016/j.conbuildmat.2021.124850.
[27] Wang L, Li G, He C, Tang Y, Yi B. Preparation and properties of nano-carbon black modified ultra-high-performance concrete. Case Stud Constr Mater 2022;17:e01378. https://doi.org/10.1016/j.cscm.2022.e01378.
[28] Dehghanpour H, Yilmaz K, Ipek M. Evaluation of recycled nano carbon black and waste erosion wires in electrically conductive concretes. Constr Build Mater 2019;221:109–21. https://doi.org/10.1016/j.conbuildmat.2019.06.025.
[29] Gao F, Tian W, Wang Z, Wang F. Effect of diameter of multi-walled carbon nanotubes on mechanical properties and microstructure of the cement-based materials. Constr Build Mater 2020;260:120452. https://doi.org/10.1016/j.conbuildmat.2020.120452.
[30] Hassan A, Elkady H, Shaaban IG. Effect of adding carbon nanotubes on corrosion rates and steel-concrete bond. Sci Rep 2019;9:1–12. https://doi.org/10.1038/s41598-019-42761-2.
[31] Pathak SS, Vesmawala GR. Effect of nano TiO2 on mechanical properties and microstructure of concrete. Mater Today Proc 2022;65:1915–21. https://doi.org/10.1016/j.matpr.2022.05.161.
[32] Ren J, Lai Y, Gao J. Exploring the influence of SiO2 and TiO2 nanoparticles on the mechanical properties of concrete. Constr Build Mater 2018;175:277–85. https://doi.org/10.1016/j.conbuildmat.2018.04.181.
[33] Santos RF, Ribeiro JCL, Franco de Carvalho JM, Magalhães WLE, Pedroti LG, Nalon GH, et al. Nanofibrillated cellulose and its applications in cement-based composites: a review. Constr Build Mater 2021;288:123122. https://doi.org/10.1016/j.conbuildmat.2021.123122.
[34] Mejdoub R, Hammi H, Suñol JJ, Khitouni M, Mnif A, Boufi S. Nanofibrillated cellulose as nanoreinforcement in Portland cement: thermal, mechanical and microstructural properties. J Compos Mater 2016;51:2491–503. https://doi.org/10.1177/0021998316672090.
[35] Hoyos CG, Vazquez A. Carbon dioxide sequestration in Portland cement paste modified with cellulose microcrystalline. In: Polar Arct. Sci. Technol. Offshore Geotech. Pet. Technol. Symp., vol. 6. American Society of Mechanical Engineers; 2013. p. 1–8. https://doi.org/10.1115/OMAE2013-11528.
[36] Zhong T, Jian G, Chen Z, Wolcott M, Nassiri S, Fernandez CA. Interfacial interactions and reinforcing mechanisms of cellulose and chitin nanomaterials and starch derivatives for cement and concrete strength and durability enhancement: a review. Nanotechnol Rev 2022;11:2673–713. https://doi.org/10.1515/ntrev-2022-0149.
[37] Cao Y, Zavaterri P, Youngblood J, Moon R, Weiss J. The influence of cellulose nanocrystal additions on the performance of cement paste. Cem Concr Compos 2015;56:73–83. https://doi.org/10.1016/j.cemconcomp.2014.11.008.
[38] Peters SJ, Rushing TS, Landis EN, Cummins TK. Nanocellulose and microcellulose fibers for concrete. Transp Res Rec 2010:25–8. https://doi.org/10.3141/2142-04.
[39] Ardanuy M, Claramunt J, Pares F, Aracri E, Vidal T. Nanofibrillated cellulose (NFC) as reinforcement for high performance cement mortar composites. Bioresources 2012;7:3883–94. https://doi.org/10.15376/biores.7.3.3883-3894.
[40] Stanislas TT, Komadja GC, Nafu YR, Mahamat AA, Mejouyo PWH, Tendo JF, et al. Potential of raffia nanofibrillated cellulose as a reinforcement in extruded earth-based materials. Case Stud Constr Mater 2022;16. https://doi.org/10.1016/j.cscm.2022.e00926.
[41] de Souza LO, Liebscher M, de Souza LMS, de Andrade Silva F, Mechtcherine V. Effect of microcrystalline and nano-fibrillated cellulose on the mechanical behavior and microstructure of cement pastes. Constr Build Mater 2023;408:8–11. https://doi.org/10.1016/j.conbuildmat.2023.133812.
[42] Dai H, Jiao L, Zhu Y, Pi C. Nanometer cellulose fiber reinforced cement-based material. Patent Publication No. PaCN105174768A; 2015.
[43] Claramunt J, Ventura H, Toledo Filho RD, Ardanuy M. Effect of nanocelluloses on the microstructure and mechanical performance of CAC cementitious matrices. Cement Concr Res 2019;119:64–76. https://doi.org/10.1016/j.cemconres.2019.02.006.
[44] Sun X, Wu Q, Lee S, Qing Y, Wu Y. Cellulose nanofibers as a modifier for rheology, curing and mechanical performance of oil well cement. Sci Rep 2016;6:1–9. https://doi.org/10.1038/srep31654.
[45] Nassiri S, Chen Z, Jian G, Zhong T, Haider MM, Li H, et al. Comparison of unique effects of two contrasting types of cellulose nanomaterials on setting time, rheology, and compressive strength of cement paste. Cem Concr Compos 2021;123:104201. https://doi.org/10.1016/j.cemconcomp.2021.104201.
[46] Kong Y, Qian S, Zhang Z, Tian J. The impact of esterified nanofibrillated cellulose content on the properties of thermoplastic starch/PBAT biocomposite films through ball-milling. Int J Biol Macromol 2023;253:127462. https://doi.org/10.1016/j.ijbiomac.2023.127462.
[47] Tian J, Kong Y, Qian S, Zhang Z, Xia Y, Li Z. Mechanically robust multifunctional starch films reinforced by surface-tailored nanofibrillated cellulose. Compos Part B Eng 2024;275:111339. https://doi.org/10.1016/j.compositesb.2024.111339.
[48] Zhang Z, Qian S, Li X, Zhu C, Li Z. Preparation of environmentally friendly ionic liquids-toughened polylactic acid/nanofibrillated cellulose composites with high

strength and precipitation resistance. Chem Eng J 2024;499:156670. https://doi.org/10.1016/j.cej.2024.156670.
[49] Oliveira de Souza L, Cordazzo M, Silva de Souza LM, Tonoli G, de Andrade Silva F, Mechtcherine V. Investigation of dispersion methodologies of microcrystalline and nano-fibrillated cellulose on cement pastes. Cem Concr Compos 2022;126. https://doi.org/10.1016/j.cemconcomp.2021.104351.
[50] Noltingk BE, Neppiras EA. Cavitation produced by ultrasonics. Proc Phys Soc B 1950;63:674–85. https://doi.org/10.1088/0370-1301/63/9/305.
[51] Huang YY, Terentjev EM. Dispersion of carbon nanotubes: Mixing, sonication, stabilization, and composite properties. Polymers 2012;4:275–95. https://doi.org/10.3390/polym4010275.
[52] Jiao L, Su M, Chen L, Wang Y, Zhu H, Dai H. Natural cellulose nanofibers as sustainable enhancers in construction cement. PLoS One 2016;11:1–13. https://doi.org/10.1371/journal.pone.0168422.
[53] Onuaguluchi O, Panesar DK, Sain M. Properties of nanofibre reinforced cement composites. Constr Build Mater 2014;63:119–24. https://doi.org/10.1016/j.conbuildmat.2014.04.072.
[54] Associação Brasileira de Normas Técnicas - ABNT. NBR 16697: Cimento Portland - Requisitos. 2018. Rio de Janeiro.
[55] Associação Brasileira de Normas Técnicas - ABNT. NBR 16605: Cimento Portland e outros materiais em pó - Determinação da massa específica. 2017. Rio de Janeiro.
[56] Sun J, Luo S, Wang Y, Dong Q, Zhang Z. Pre-treatment of steel slag and its applicability in asphalt mixtures for sustainable pavements. Chem Eng J 2023;476:146802. https://doi.org/10.1016/j.cej.2023.146802.
[57] Song Q, Guo MZ, Wang L, Ling TC. Use of steel slag as sustainable construction materials: a review of accelerated carbonation treatment. Resour Conserv Recycl 2021;173:105740. https://doi.org/10.1016/j.resconrec.2021.105740.
[58] Sasaki T, Hamazaki T. Development of steam-aging process for steel slag. Nippon Steel Sumitomo Met Tech Rep 2015:23–6.
[59] Martins ACP, Franco de Carvalho JM, Duarte M do N, Lima GES de, Pedroti LG, Peixoto RAF. Influence of a LAS-based modifying admixture on cement-based composites containing steel slag powder. J Build Eng 2022;53. https://doi.org/10.1016/j.jobe.2022.104517.
[60] Viana LC, De Muniz GIB, Magalhães WLE. Propriedades físicas e mecânicas de filmes nanoestruturados obtidos a partir de polpa Kraft de Pinus sp. não branqueada. Sci Sci 2017;45:653–62. https://doi.org/10.18671/scifor.v45n116.06.
[61] Parveen S, Rana S, Fangueiro R, Paiva MC. A novel approach of developing micro crystalline cellulose reinforced cementitious composites with enhanced microstructure and mechanical performance. Cem Concr Compos 2017;78:146–61. https://doi.org/10.1016/j.cemconcomp.2017.01.004.
[62] Associação Brasileira de Normas Técnicas - ABNT. NBR 16974: Agregado graúdo - Ensaio de abrasão Los Angeles. Rio de Janeiro; 2021.
[63] Funk JE, Dinger DA. Particle size control for high-solids castable refractories. Am Ceram Soc Bull 1994;73:66–9.
[64] Snehal K, Das BB. Application of andreassen and modified Andreassen model on cementitious mixture design: a review. Adv. Sci. Technol. Innov. 2021:729–50. https://doi.org/10.1007/978-981-15-4577-1_63.
[65] Kamasamudram KS, Ashraf W, Landis EN. Cellulose nanocomposites for performance enhancement of ordinary Portland cement-based materials. Transp Res Rec J Transp Res Board 2020:036119812095842. https://doi.org/10.1177/0361198120958421.
[66] Sharma A, Mandal T, Goswami S. Dispersibility and stability studies of cellulose nanofibers: implications for nanocomposite preparation. J Polym Environ 2021;29:1516–25. https://doi.org/10.1007/s10924-020-01974-7.
[67] Parveen S, Rana S, Ferreira S, Filho A, Fangueiro R. Ultrasonic dispersion of micro crystalline cellulose for developing cementitious composites with excellent strength and stiffness. Ind Crops Prod 2018;122:156–65. https://doi.org/10.1016/j.indcrop.2018.05.060.
[68] Kantro D. Influence of water-reducing admixtures on properties of cement paste—a miniature slump test. Cem Concr Aggregates 1980;2:95. https://doi.org/10.1520/CCA10190J.
[69] Scrivener K, Snellings R, Lothenbach B, editors. A practical Guide to microstructural analysis of cementitious materials. Boca Raton: CRC Press; 2018. https://doi.org/10.1201/b19074.
[70] Associação Brasileira de Normas Técnicas - ABNT. NBR 13279: Argamassas para assentamento e revestimento de paredes e tetos - Determinação da resistência à tração na flexão e à compressão. Rio de Janeiro; 2005.
[71] ASTM. Astm C348-20: standard test method for flexural strength of hydraulic-cement mortars, vol. 3; 2014. https://doi.org/10.1520/C0348-14.2.
[72] ASTM. Astm C349-18: standard test method for compressive strength of hydraulic-cement mortars (using portions of prisms broken in flexure). 2018. https://doi.org/10.1520/C0348-14.2.
[73] Damineli BL, Kemeid FM, Aguiar PS, John VM. Measuring the eco-efficiency of cement use. Cem Concr Compos 2010;32:555–62. https://doi.org/10.1016/j.cemconcomp.2010.07.009.
[74] Damineli BL, Pileggi RG, John VM. Lower binder intensity eco-efficient concretes. In: Pacheco-Torgal F, Jalali S, Labrincha J, John VM, editors. Eco-efficient Concr. Elsevier; 2013. p. 26–44. https://doi.org/10.1533/9780857098993.1.26.
[75] Coura MR, Demuner AJ, Ribeiro RA, Demuner IF, de Cristo Figueiredo J, Gomes FJB, et al. Microfibrillated celluloses produced from kraft pulp of coffee parchment. Biomass Convers Biorefinery 2024. https://doi.org/10.1007/s13399-024-06024-z.
[76] Correia V da C, Santos SF, Soares Teixeira R, Savastano Junior H. Nanofibrillated cellulose and cellulosic pulp for reinforcement of the extruded cement based materials. Constr Build Mater 2018;160:376–84. https://doi.org/10.1016/j.conbuildmat.2017.11.066.
[77] Chen Zhebo, Deutsch Todd G, Dinh Huyen N, Domen Kazunari, Emery Keith, Forman Arnold J, Gaillard Nicolas, Garland Roxanne, Heske Clemens, Jaramillo Thomas F, Kleiman-Shwarsctein Alan, Eric Miller KT, Jt. UV-vis spectroscopy. In: Chen Z, Dinh HN, Miller E, editors. Photoelectrochem. Water Split. New York, NY: Springer New York; 2013. p. 126. https://doi.org/10.1007/978-1-4614-8298-7.
[78] Dumée L, Sears K, Schütz J, Finn N, Duke M, Gray S. Influence of the sonication temperature on the debundling kinetics of carbon nanotubes in propan-2-ol. Nanomaterials 2013;3:70–85. https://doi.org/10.3390/nano3010070.
[79] Foster EJ, Moon RJ, Agarwal UP, Bortner MJ, Bras J, Camarero-Espinosa S, et al. Current characterization methods for cellulose nanomaterials. Chem Soc Rev 2018;47:2609–79. https://doi.org/10.1039/c6cs00895j.
[80] Balea A, Fuente E, Blanco A, Negro C. Nanocelluloses: natural-based materials for fiber-reinforced cement composites. A critical review. Polymers 2019;11:518. https://doi.org/10.3390/polym11030518.
[81] Wang Q, Yan P. Hydration properties of basic oxygen furnace steel slag. Constr Build Mater 2010;24:1134–40. https://doi.org/10.1016/j.conbuildmat.2009.12.028.
[82] Franco de Carvalho JM, Defáveri K, Mendes JC, Schmidt W, Kühne H-C, Peixoto RAF. Influence of particle size-designed recycled mineral admixtures on the properties of cement-based composites. Constr Build Mater 2021;272:121640. https://doi.org/10.1016/j.conbuildmat.2020.121640.
[83] Martins ACP, Franco de Carvalho JM, Costa LCB, Andrade HD, de Melo TV, Ribeiro JCL, et al. Steel slags in cement-based composites: an ultimate review on characterization, applications and performance. Constr Build Mater 2021;291:123265. https://doi.org/10.1016/j.conbuildmat.2021.123265.
[84] Grazia MT De. Short and long-term performance of eco-efficient concrete mixtures. University of Ottawa; 2023.